Band-offset ratio dependence on the effective-mass Hamiltonian based on a modified profile of the GaAs-$Al_xGa_{1-x}As$ quantum well

Tsung L. Li and Kelin J. Kuhn
Department of Electrical Engineering, FT-10, University of Washington, Seattle, Washington 98195
(Received 22 October 1991; revised manuscript received 3 December 1992)

This paper suggests a simple permutation scheme to construct the Hermitian Hamiltonian utilized in the effective-mass equation, introduces a smoothed profile to more accurately model heterojunctions, and illustrates the dependence of the band-offset ratio of a GaAs-$Al_xGa_{1-x}As$ quantum well on the particular Hermitian Hamiltonian used in the calculation. The permutation scheme produces the BenDaniel and Duke Hamiltonian, the Bastard Hamiltonian, the Zhu and Kroemer Hamiltonian, and a Hamiltonian termed the redistributed Hamiltonian in this paper. The heterojunction is modeled by an error function rather than a step function to more accurately model the material transition region at the interface between the two materials. The 11 heavy-hole (HH) transition energy obtained by BenDaniel and Duke Hamiltonian with a particular band-offset ratio is reproduced by utilizing non-BenDaniel and Duke Hamiltonians with appropriate band-offset ratios. This process is repeated for BenDaniel and Duke Hamiltonian band-offset ratios varying from 0.5 to 0.8, and then proceeds to 11 light-hole (LH), 22 HH, and 22 LH transitions. It is found that the Hamiltonian dependence of the band-offset ratio is significant.

I. INTRODUCTION

The conduction-band-offset ratio, which is the ratio of the conduction-band offset to the total band gap of the heterojunction, has been investigated in GaAs-$Al_xGa_{1-x}As$ quantum wells because of its fundamental importance and application. The ratio has been measured by spectroscopic[1-6] and electrical[7-9] methods, and the reported value ranges from 0.88 to 0.57. From Duggan's[10] and Kroemer's[11] review articles about the experimental and theoretical work, it can be seen that spectroscopic techniques are preferred over electrical ones in exploring the band-offset ratio via a quantum well, and that researchers using spectroscopy usually try to match their data with the theoretical results to determine the band offset.

Recently, there have been many computational works discussing the band-offset ratio by using the first-principles approach.[12-14] These calculations are usually based on the microscopic atomic arrangement at the interface. In these calculations, the potential energy consists of three contributions: the ionic, the Hartree, and the exchange potentials. On the other hand, the effective-mass approach assumes a macroscopic position-dependent potential and an effective-mass Hamiltonian.[15]

There is no unique representation of the kinetic-energy operator of the single-band effective-mass Hamiltonian in the effective-mass approach.[16,17] Three frequently used Hermitian Hamiltonians found in the literature are the BenDaniel and Duke Hamiltonian,[18] the Bastard Hamiltonian,[16,19] and the Zhu and Kroemer Hamiltonian.[20] In this paper, these Hamiltonians will be shown to be obtainable by a simple permutation scheme, and this scheme suggests another Hermitian Hamiltonian termed the redistributed Hamiltonian in this paper.

As to the macroscopic potential of a square quantum well, the position-dependent potential is frequently modeled by a discontinuous profile, namely, a step function.[1,2,4,6] However, in this paper, the step change of the profile is replaced by an error function because, in the real world, neither the potential nor the effective mass can change abruptly across the heterojunction.

In the work published by Chomette *et al.* in 1986,[21] it was shown that the band-offset ratio depends on the analytic model and the interface conditions employed to compute the transition energy. This observation initiates an inquiry about the dependence of the band-offset ratio on the Hamiltonian used in the effective-mass equation, and it is this dependence which will be studied in this paper.

First, based on the smoothed profile, the transition levels in the conduction band are calculated to illustrate the effects of the modified profile; and second, the band-offset ratios required for the quantum well to yield the same 11 heavy-hole (HH), 11 light-hole (LH), 22 HH, and 22 LH transition energies are computed by using four different Hamiltonians. The transitions of $n=1(c)$ to $n=1$ (hh), $n=1(c)$ to $n=1$(lh), $n=2(c)$ to $n=2$(hh), and $n=2(c)$ to $n=2$(lh) are denoted by 11 HH, 11 LH, 22 HH, and 22 LH, respectively. This paper reveals the notable Hamiltonian dependence of the band-offset ratio when the quantum well with a modified profile is utilized.

II. EFFECTIVE-MASS HAMILTONIANS

The single-band effective-mass approach to a quantum-well problem requires that the envelope function ψ satisfy the effective-mass equation

$$\hat{H}\psi = E\psi \ , \tag{1}$$

where E is the energy eigenvalue and $\hat{H}$ is the Hamiltonian operator consisting of the kinetic-energy operator ($\hat{T}$)

and the potential-energy operator ($\hat{V}$),

$$\hat{H}=\hat{T}(\hat{z})+\hat{V}(\hat{z}) . \tag{2}$$

Due to the compositional variation in a quantum well as a function of location, the kinetic energy and the potential energy are expressed as position-dependent operators in Eq. (2).

The kinetic-energy operator can be considered to be composed of four elements: $1/\sqrt{m(\hat{z})}$, $1/\sqrt{m(\hat{z})}$, $\hat{p}$, and $\hat{p}$, where $\hat{z}$ and $\hat{p}$ are position and momentum operators, respectively. Because $1/\sqrt{m(\hat{z})}$ and $\hat{p}$ are not commutable, there are six possible permutations to represent the kinetic-energy operator:

$$\hat{T}_1(\hat{z})=\tfrac{1}{2}\hat{p}\hat{p}\frac{1}{\sqrt{m(\hat{z})}}\frac{1}{\sqrt{m(\hat{z})}}=\tfrac{1}{2}\hat{p}^2\frac{1}{m(\hat{z})} , \tag{3}$$

$$\hat{T}_2(\hat{z})=\tfrac{1}{2}\hat{p}\frac{1}{\sqrt{m(\hat{z})}}\hat{p}\frac{1}{\sqrt{m(\hat{z})}}=\tfrac{1}{2}\hat{p}\frac{1}{\sqrt{m(\hat{z})}}\hat{p}\frac{1}{\sqrt{m(\hat{z})}} , \tag{4}$$

$$\hat{T}_3(\hat{z})=\tfrac{1}{2}\hat{p}\frac{1}{\sqrt{m(\hat{z})}}\frac{1}{\sqrt{m(\hat{z})}}\hat{p}=\tfrac{1}{2}\hat{p}\frac{1}{m(\hat{z})}\hat{p} , \tag{5}$$

$$\hat{T}_4(\hat{z})=\frac{1}{2}\frac{1}{\sqrt{m(\hat{z})}}\hat{p}\hat{p}\frac{1}{\sqrt{m(\hat{z})}}=\frac{1}{2}\frac{1}{\sqrt{m(\hat{z})}}\hat{p}^2\frac{1}{\sqrt{m(\hat{z})}} , \tag{6}$$

$$\hat{T}_5(\hat{z})=\frac{1}{2}\frac{1}{\sqrt{m(\hat{z})}}\hat{p}\frac{1}{\sqrt{m(\hat{z})}}\hat{p}=\frac{1}{2}\frac{1}{\sqrt{m(\hat{z})}}\hat{p}\frac{1}{\sqrt{m(\hat{z})}}\hat{p} , \tag{7}$$

and

$$\hat{T}_6(\hat{z})=\frac{1}{2}\frac{1}{\sqrt{m(\hat{z})}}\frac{1}{\sqrt{m(\hat{z})}}\hat{p}\hat{p}=\frac{1}{2}\frac{1}{m(\hat{z})}\hat{p}^2 . \tag{8}$$

Of the six kinetic energy operators, only two are Hermitian: $\hat{T}_3(\hat{z})$ and $\hat{T}_4(\hat{z})$. The third permutation $\hat{T}_3(\hat{z})$ is the kinetic-energy part of the Hamiltonian proposed by BenDaniel and Duke,[18]

$$\hat{H}_{\mathrm{BDD}}=\tfrac{1}{2}\hat{p}\frac{1}{m(\hat{z})}\hat{p}+V(\hat{z}) . \tag{9}$$

The fourth permutation $\hat{T}_4(\hat{z})$ is the kinetic-energy term of the Hamiltonian suggested by Zhu and Kroemer,[20]

$$\hat{H}_{\mathrm{ZK}}=\frac{1}{2}\frac{1}{\sqrt{m(\hat{z})}}\hat{p}^2\frac{1}{\sqrt{m(\hat{z})}}+V(\hat{z}) . \tag{10}$$

The rest of four kinetic-energy operators, $\hat{T}_1(\hat{z})$, $\hat{T}_2(\hat{z})$, $\hat{T}_5(\hat{z})$, and $\hat{T}_6(\hat{z})$ are not Hermitian. However, they constitute two adjoint pairs, namely, $\hat{T}_1(\hat{z})=\hat{T}_6(\hat{z})^\dagger$ and $\hat{T}_2(\hat{z})=\hat{T}_5(\hat{z})^\dagger$. Hermiticity can, therefore, be achieved by averaging the adjoint kinetic-energy operator pair.

The average of $\hat{T}_1(\hat{z})$ and $\hat{T}_6(\hat{z})$ is the kinetic-energy operator of the Hamiltonian first proposed by Gora and Williams,[16] but it is frequently termed the Bastard Hamiltonian,[19]

$$\hat{H}_B=\frac{1}{4}\left[\hat{p}^2\frac{1}{m(\hat{z})}+\frac{1}{m(\hat{z})}\hat{p}^2\right]+V(\hat{z}) . \tag{11}$$

Similarly, the average of $\hat{T}_2(\hat{z})$ and $\hat{T}_5(\hat{z})$ results in the kinetic-energy portion of an additional Hamiltonian,

$$\hat{H}_R=\frac{1}{4}\left[\hat{p}\frac{1}{\sqrt{m(\hat{z})}}\hat{p}\frac{1}{\sqrt{m(\hat{z})}}+\frac{1}{\sqrt{m(\hat{z})}}\hat{p}\frac{1}{\sqrt{m(\hat{z})}}\hat{p}\right]+V(\hat{z}) . \tag{12}$$

In comparison with the existing Hamiltonians, the mass operators of this Hamiltonian are redistributed among the momentum terms. Thus it is called the redistributed Hamiltonian in this paper.

The single-band effective mass Hamiltonians given in Eqs. (9)–(12) are special cases of a general form of the Hamiltonian introduced by von Roos,[22,17]

$$\hat{H}_{\mathrm{vR}}=\tfrac{1}{4}[m(\hat{z})^\alpha\hat{p}m(\hat{z})^\beta\hat{p}m(\hat{z})^\gamma+m(\hat{z})^\gamma\hat{p}m(\hat{z})^\beta\hat{p}m(\hat{z})^\alpha]+V(\hat{z}) , \tag{13}$$

where $\alpha+\beta+\gamma=-1$. In works by Morrow and Brownstein[17] and Thomsen, Einevoll, and Hemmer,[23] it is demonstrated that the Bastard Hamiltonian and the redistributed Hamiltonian are not valid if the heterojunction has an abrupt mass profile. Because a gradually varying mass profile will be assumed in the next section, these two Hamiltonians shall not be excluded from this paper.

The form of the effective-mass Hamiltonian has been a controversial subject due to the location dependence of the effective mass. Morrow has a good review on this subject in his work published in 1987.[24] Recently, there has been growing consensus in favor of the BenDaniel and Duke Hamiltonian, for instance, the theoretical work by Burt,[25,26] the examination of heterojunctions in three dimensions by Morrow,[27] the exact treatment of a δ well in one dimension by Thomsen, Einevoll, and Hemmer,[23] the solution to a one-dimensional Kronig-Penney lattice by Einevoll and Hemmer,[28] and the low-temperature photoluminescence data published by Galbraith and Duggan.[29]

By the correspondence in wave mechanics $\hat{p}\rightarrow -i\hbar d/dz$ and $\hat{z}\rightarrow z$, the effective-mass equation (1) together with any of the four Hamiltonians given in Eqs. (9)–(12) can be written in a differential form,

$$-\frac{\hbar^2}{2}\frac{d}{dz}\left[\frac{1}{m(z)}\frac{d\psi(z)}{dz}\right]+V^{\mathrm{eff}}(z)\psi(z)=E\psi(z) , \tag{14}$$

where $V^{\mathrm{eff}}(z)$ is termed the effective potential energy whose algebraic form depends on the Hamiltonian employed. For the BenDaniel and Duke Hamiltonian,

$$V^{\mathrm{eff}}(z)=V^{\mathrm{eff}}_{\mathrm{BDD}}(z)=V(z) . \tag{15}$$

For the redistributed Hamiltonian proposed in Eq. (12),

$$V^{\text{eff}}(z)=V_R^{\text{eff}}(z)$$
$$=-\frac{\hbar^2}{2}\frac{1}{m(z)^3}[\tfrac{1}{2}m'(z)^2-\tfrac{1}{4}m(z)m''(z)]+V(z)\ . \tag{16}$$

For the Bastard Hamiltonian,

$$V^{\text{eff}}(z)=V_B^{\text{eff}}(z)$$
$$=-\frac{\hbar^2}{2}\frac{1}{m(z)^3}[m'(z)^2-\tfrac{1}{2}m(z)m''(z)]+V(z)\ . \tag{17}$$

For the Zhu and Kroemer Hamiltonian,

$$V^{\text{eff}}(z)=V_{\text{ZK}}^{\text{eff}}(z)$$
$$=-\frac{\hbar^2}{2}\frac{1}{m(z)^3}[\tfrac{3}{4}m'(z)^2-\tfrac{1}{2}m(z)m''(z)]+V(z)\ . \tag{18}$$

The first and second derivatives of $m(z)$ with respect to z are denoted by $m'(z)$ and $m''(z)$. As shown in Eqs. (15)–(18), the effective potential is, in fact, the sum of the real potential profile $V(z)$ and the modification emerged from the location dependence of the effective mass. A different Hamiltonian leads to a different modification term.

All of the effective potentials given in Eqs. (15)–(18) can be summarized in a general form of the effective potential,

$$V^{\text{eff}}(z)=-\frac{\hbar^2}{2}\frac{1}{m(z)^3}[am'(z)^2-bm(z)m''(z)]+V(z)\ , \tag{19}$$

where the coefficients a and b depend on the Hamiltonian and are tabulated in Table I.

The general form of the Hamiltonian given in Eq. (13) can also be written in a differential form such as Eq. (14), with the effective potential given by Eq. (19). But the coefficients a and b are related to α, β, and γ by

$$a=1+\beta-\alpha\gamma \tag{20}$$

and

$$b=\tfrac{1}{2}(1+\beta)\ . \tag{21}$$

If α, β, and γ take the values given in the last three columns of Table I, the von Roos Hamiltonian reduces to the Hamiltonian listed in the first column of the table.

TABLE I. Single-band effective-mass Hamiltonians. The coefficients a and b of the effective potential given in Eq. (19) depend on the Hamiltonian used for the effective-mass equation. The BenDaniel and Duke Hamiltonian, the redistributed Hamiltonian, the Bastard Hamiltonian, and the Zhu and Kroemer Hamiltonian are special cases of the von Roos Hamiltonian in Eq. (13), when the exponents, α, β, and γ listed in the last three columns of the table are utilized.

Hamiltonian	a	b	α	β	γ
BenDaniel and Duke	0	0	0	−1	0
Redistributed	$\frac{1}{2}$	$\frac{1}{4}$	0	$-\frac{1}{2}$	$-\frac{1}{2}$
Bastard	1	$\frac{1}{2}$	−1	0	0
Zhu and Kroemer	$\frac{3}{4}$	$\frac{1}{2}$	$-\frac{1}{2}$	0	$-\frac{1}{2}$

III. MODIFIED SQUARE QUANTUM WELL

A square quantum well subject to no external field is usually modeled by a step profile which is discontinuous at the heterojunctions. The commonly used interface conditions at the heterojunctions are (1) the continuity of the envelope function and its first derivative, or (2) the continuity of the envelope function and its first derivative divided by the effective mass.

Within each flat region of the square quantum well, the mass is a constant, and the effective potentials of the four Hamiltonians given in Eqs. (15)–(18) are identical because the derivatives of the mass with respect to the position vanish. Thus envelope functions within each flat region are independent of the Hamiltonian used for the analysis. If the same interface conditions at the discontinuous points between two adjacent regions are essentially imposed for the four Hamiltonians, the eigensolutions will be exactly identical.[30] As a result, the four Hamiltonians produce the same transition energy, namely, the band-offset ratio will be independent of the Hamiltonian if the heterojunction is modeled by a step function with essentially imposed interface conditions.

However, the discontinuity of the square quantum-well model implies an infinite internal electric field at the heterojunctions, and this is not physically possible. In reality, the potential changes over a few monolayers for a perfect microscopic interface. Stern and Sarma[31] have investigated the gradually varying interface potential of a modulation-doped heterojunction. In this paper, the square quantum well is modeled by a smoothed profile and it is termed a modified square quantum well. The heterojunction is simulated by an error function rather than a step function, hence, the effective potential $V^{\text{eff}}(z)$ differs for distinct Hamiltonians. The modified potential profile is illustrated in Fig. 1 by the solid line, which removes the discontinuity of the sharp square quantum well. (The rest of the curves in the figure will be explained in Appendix A.)

In this paper, the quantum well is fabricated by GaAs and $Al_xGa_{1-x}As$ in the [001] direction, where x is the composition fraction of Al. For $Al_xGa_{1-x}As$ with $0\le x\le 0.45$, the band-gap energy, the effective mass of the electron in the conduction band, and the effective masses of the heavy and light holes in the valence band take the following relations:[32,33,15]

$$E_g(Al_xGa_{1-x}As)=\delta+\nu x\ , \tag{22}$$

$$m_e(Al_xGa_{1-x}As)=\alpha_e+\mu_e x\ , \tag{23}$$

$$m_{\text{hh}}(Al_xGa_{1-x}As)=\alpha_{\text{hh}}+\mu_{\text{hh}}x\ , \tag{24}$$

and

$$m_{\text{lh}}(Al_xGa_{1-x}As)=\alpha_{\text{lh}}+\mu_{\text{lh}}x\ , \tag{25}$$

where $\delta=1.424$ eV, $\nu=1.247$ eV, $\alpha_e=0.067m_0$,

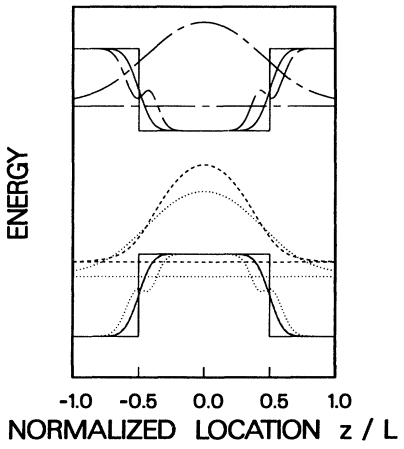

FIG. 1. A modified square quantum well manufactured by GaAs and $Al_{0.3}Ga_{0.7}As$ with a conduction-band-offset ratio of 0.5 is illustrated. The step profiles in solid line segments are the profiles commonly used; the smooth profiles in solid curves are the modified profiles utilized in this paper. The effective potentials of the Zhu and Kroemer Hamiltonian are depicted. Only the envelope functions of the first eigenlevels are plotted, in spite of the fact that there are two, three, and two levels for the electron, the heavy hole, and the light hole, respectively. The envelope functions and the effective potentials of the electron and the heavy and light holes are drawn in chain-dashed, dashed, and dotted curves, respectively.

$\mu_e=0.083m_0$, $\alpha_{hh}=0.35m_0$, $\mu_{hh}=0.05m_0$, $\alpha_{lh}=0.08m_0$, and $\mu_{lh}=0.10m_0$. The free-electron mass is denoted by m_0.

In the conduction band, the electron effective mass and the potential energy of the modified square quantum well are given by

$$m_e(z)=\alpha_e+\frac{\beta_e}{2}\left\{1+\mathrm{erf}\left[\frac{1}{\sqrt{2}\sigma_e}\left[|z|-\frac{L}{2}\right]\right]\right\} \tag{26}$$

and

$$V_C(z)=\frac{V_C^0}{2}\left\{1+\mathrm{erf}\left[\frac{1}{\sqrt{2}\sigma_C}\left[|z|-\frac{L}{2}\right]\right]\right\}, \tag{27}$$

with

$$V_C^0=\nu x Q_C \tag{28}$$

and

$$\beta_e=\mu_e x\ , \tag{29}$$

where L is the quantum-well width, which is the separation between the two inflection points of the modified profile, and where σ_e and σ_C are the dispersive factors which designate the change rates of the electron effective mass and conduction-band potential energy at the heterojunctions. The first derivatives of the mass and the potential profiles, for either $z>0$ or $z<0$, are normally distributed with standard deviations of σ_e and σ_C, respectively. The error function is defined by $\mathrm{erf}(t)=2/\sqrt{\pi}\int_0^t \exp(-s^2)ds$. The conduction-band-offset ratio is denoted by Q_C and its relation to the conduction-band-offset energy is $V_C^0=Q_C\Delta E_g$, where ΔE_g is the band-gap difference between $Al_xGa_{1-x}As$ and GaAs, and $\Delta E_g=\nu x$. Recall that x is the composition fraction of Al in the barrier.

The first and second derivatives of the mass are essential to the calculation of the effective potential in Eq. (19). They are given below:

$$m_e'(z)=\begin{cases}\beta_e/\sqrt{2\pi}\sigma_e\exp[-(z-L/2)^2/2\sigma_e^2] & \text{if } z>0\\ -\beta_e/\sqrt{2\pi}\sigma_e\exp[-(z+L/2)^2/2\sigma_e^2] & \text{if } z<0\end{cases} \tag{30}$$

and

$$m_e''(z)=\begin{cases}-(z-L/2)\beta_e/\sqrt{2\pi}\sigma_e^3\exp[-(z-L/2)^2/2\sigma_e^2] & \text{if } z>0\\ (z+L/2)\beta_e/\sqrt{2\pi}\sigma_e^3\exp[-(z+L/2)^2/2\sigma_e^2] & \text{if } z<0\ .\end{cases} \tag{31}$$

Rigorously speaking, the first derivative of the mass is discontinuous at the origin; that is, the mass is a C^0 function. The slope discontinuity normalized by the ratio of the characteristic mass (m_0) and the characteristic length (L) reads

$$\frac{m_e'(0^+)-m_e'(0^-)}{m_0/L}=\frac{2\beta_e/m_0}{\sqrt{2\pi}(\sigma_e/L)}\exp\left[-\frac{1}{8(\sigma_e/L)^2}\right]. \tag{32}$$

Similarly, in the valence band, the effective masses of the heavy and the light holes and the potential energy are given by

$$m_{hh}(z)=\alpha_{hh}+\frac{\beta_{hh}}{2}\left\{1+\mathrm{erf}\left[\frac{1}{\sqrt{2}\sigma_{hh}}\left[|z|-\frac{L}{2}\right]\right]\right\}, \tag{33}$$

$$m_{lh}(z)=\alpha_{lh}+\frac{\beta_{lh}}{2}\left\{1+\mathrm{erf}\left[\frac{1}{\sqrt{2}\sigma_{lh}}\left[|z|-\frac{L}{2}\right]\right]\right\} \tag{34}$$

and

$$V_V(z)=\frac{V_V^0}{2}\left\{1+\mathrm{erf}\left[\frac{1}{\sqrt{2}\sigma_V}\left[|z|-\frac{L}{2}\right]\right]\right\}, \tag{35}$$

with

$$V_V^0=\nu x Q_V , \tag{36}$$

$$\beta_{\mathrm{hh}}=\mu_{\mathrm{hh}}x , \tag{37}$$

and

$$\beta_{\mathrm{lh}}=\mu_{\mathrm{lh}}x , \tag{38}$$

where σ_{hh}, σ_{lh}, and σ_V are the dispersive factors which characterize the change rates of the effective masses of the heavy and light holes and the valence-band potential energy at heterojunctions. Q_V is the valence-band-offset ratio and $Q_C+Q_V=1$. From Eqs. (29), (37), and (38), note that $\beta_e/\mu_e=\beta_{\mathrm{hh}}/\mu_{\mathrm{hh}}=\beta_{\mathrm{lh}}/\mu_{\mathrm{lh}}=x$.

The first and second derivatives of the masses of the heavy and the light holes, and the discontinuity of their first derivatives at $z=0$, are similar to those of the electron. They are attainable by replacing the subscript e in Eqs. (30)–(32) by the subscript hh for the heavy hole, and by the subscript lh for the light hole.

IV. BAND-OFFSET RATIO CALCULATION

Given a modified square quantum well, the transition energy depends on the eigenenergies of the conduction and the valence bands. The eigenenergies, in turn, rely on the ratio of the conduction-band offset to the total band gap as well as on the Hamiltonian utilized in the computation. In this section, first, the methods for calculating the transition energy will be given. Second, the scheme employed to reveal the Hamiltonian dependence of the band-offset ratio will be shown.

The three-dimensional form of the general Hamiltonian suggested by von Roos in Eq. (13) is utilized to incorporate the exciton effects.[27] Assuming that both the effective mass and the permittivity are isotropic, the excitonic Hamiltonian reads[34,35]

$$\begin{aligned}\hat{H}_{\mathrm{ex}}=&\tfrac{1}{4}[m_e(\hat{z}_e)^{\alpha}\bar{p}_e m_e(\hat{z}_e)^{\beta}\bar{p}_e m_e(\hat{z}_e)^{\gamma}+m_e(\hat{z}_e)^{\gamma}\bar{p}_e m_e(\hat{z}_e)^{\beta}\bar{p}_e m_e(\hat{z}_e)^{\alpha}]\\&+\tfrac{1}{4}[m_h(\hat{z}_h)^{\alpha}\bar{p}_h m_h(\hat{z}_h)^{\beta}\bar{p}_h m_h(\hat{z}_h)^{\gamma}+m_h(\hat{z}_h)^{\gamma}\bar{p}_h m_h(\hat{z}_h)^{\beta}\bar{p}_h m_h(\hat{z}_h)^{\alpha}]\\&+V(|\bar{r}_e-\bar{r}_h|)+V_e(\hat{z}_e)+V_h(\hat{z}_h) ,\end{aligned} \tag{39}$$

with $\alpha+\beta+\gamma=-1$, where $\bar{p}_e=(\hat{p}_{e,x},\hat{p}_{e,y},\hat{p}_{e,z})$, $\bar{p}_h=(\hat{p}_{h,x},\hat{p}_{h,y},\hat{p}_{h,z})$, $\bar{r}_e=(\hat{x}_e,\hat{y}_e,\hat{z}_e)$, and $\bar{r}_h=(\hat{x}_h,\hat{y}_h,\hat{z}_h)$ are the momenta and locations operators of the electron and the hole. The operators grouped by the square brackets of Eq. (39) are the kinetic-energy operators of the electron and the hole. The confinement potentials of the electron and the hole are denoted by $V_e(\hat{z}_e)$ and $V_h(\hat{z}_h)$, respectively. If the modified profiles given in Sec. III are employed, from Eqs. (27) and (35), $V_e(\hat{z}_e)=V_C(\hat{z}_e)$ and $V_h(\hat{z}_h)=V_V(\hat{z}_h)$.

Assume that the electron and hole interact like two point charges. Then their Coulomb potential is given, in MKS units, by

$$V(|\bar{r}_e-\bar{r}_h|)=-\frac{e^2}{4\pi\epsilon[(\hat{x}_e-\hat{x}_h)^2+(\hat{y}_e-\hat{y}_h)^2+(\hat{z}_e-\hat{z}_h)^2]^{1/2}} , \tag{40}$$

where ϵ is the permittivity of the material, and e is the absolute value of the electron charge. Equations (39) and (40) are valid for both the heavy and the light holes. Hence, the subscript h can be replaced by hh for the heavy hole or by lh for the light hole, as appropriate.

Neglecting the planar translation of the mass center of the exciton, the excitonic Hamiltonian given in Eq. (39) can be expressed in a differential form:

$$\begin{aligned}H_{\mathrm{ex}}=&-\frac{\hbar^2}{2\mu(z_e,z_h)}\left[\frac{\partial^2}{\partial x^2}+\frac{\partial^2}{\partial y^2}\right]\\&-\frac{\hbar^2}{2}\frac{\partial}{\partial z_e}\left[\frac{1}{m_e(z_e)}\frac{\partial}{\partial z_e}\right]-\frac{\hbar^2}{2}\frac{\partial}{\partial z_h}\left[\frac{1}{m_h(z_h)}\frac{\partial}{\partial z_h}\right]\\&-\frac{e^2}{4\pi\epsilon[x^2+y^2+(z_e-z_h)^2]^{1/2}}\\&+V_e^{\mathrm{eff}}(z_e)+V_h^{\mathrm{eff}}(z_h) ,\end{aligned} \tag{41}$$

where $x=x_e-x_h$ and $y=y_e-y_h$ are the planar coordinates of the electron relative to the hole. The reduced mass becomes location dependent:

$$\frac{1}{\mu(z_e,z_h)}=\frac{1}{m_e(z_e)}+\frac{1}{m_h(z_h)} . \tag{42}$$

The effective potentials of the electron and the hole are obtainable by the same algebra as in Eq. (19):

$$V_e^{\mathrm{eff}}(z_e)=-\frac{\hbar^2}{2}\frac{1}{m_e(z_e)^3}[am_e'(z_e)^2-bm_e(z_e)m_e''(z_e)]+V_C(z_e) \tag{43}$$

and

$$V_h^{\text{eff}}(z_h)=-\frac{\hbar^2}{2}\frac{1}{m_h(z_h)^3}[am_h'(z_h)^2-bm_h(z_h)m_h''(z_h)] + V_V(z_h) , \quad (44)$$

where $m_e'(z_e)=dm_e(z_e)/dz_e$, $m_e''(z_e)=d^2m_e(z_e)/dz_e^2$, $m_h'(z_h)=dm_h(z_h)/dz_h$, and $m_h''(z_h)=d^2m_h(z_h)/dz_h^2$. Coefficients a and b are given in Eqs. (20) and (21).

In Fig. 8 of the paper published by Miller *et al.*,[36] the exciton binding energy is calculated for band-offset ratios of 0.57 and 0.85 by the conventional square quantum well and the variational method. As far as we can resolve from the figure, by altering the band-offset ratio from 0.57 to 0.85, the exciton binding energy at zero electric field differs by 0.04 and 0.15 meV for the heavy-hole and the light-hole exciton, respectively. In comparison with the transition-energy differences resulting from the employment of the Hamiltonians shown in Figs. 5 and 6 of this paper, these exciton binding-energy differences are an order of magnitude less. As a result, the change of the exciton binding energy due to the band-offset ratio is negligibly small in comparison with the transition-energy difference needed to be compensated for. (The compensating process will be explained in the next section.) Therefore, the interaction term of the electron and the hole is ignored in this paper. Under these circumstances, the Hamiltonian becomes

$$H=-\frac{\hbar^2}{2\mu(z_e,z_h)}\left[\frac{\partial^2}{\partial x^2}+\frac{\partial^2}{\partial y^2}\right] -\frac{\hbar^2}{2}\frac{\partial}{\partial z_e}\left[\frac{1}{m_e(z_e)}\frac{\partial}{\partial z_e}\right]-\frac{\hbar^2}{2}\frac{\partial}{\partial z_h}\left[\frac{1}{m_h(z_h)}\frac{\partial}{\partial z_h}\right] + V_e^{\text{eff}}(z_e)+V_h^{\text{eff}}(z_h) . \quad (45)$$

The eigenproblem,

$$H\Psi(x,y,z_e,z_h)=(E_T-E_G)\Psi(x,y,z_e,z_h) , \quad (46)$$

can be solved by separating variables x and y from variables z_e and z_h, where E_T and E_G are the transition energy of the system and band-gap energy of GaAs, respectively.

Noting that $\mathbf{k}_\parallel=(k_x,k_y)$ and $\mathbf{r}_\parallel=(x,y)$, the solution to Eq. (46) reads

$$\Psi(x,y,z_e,z_h)=\exp(i\mathbf{k}_\parallel\cdot\mathbf{r}_\parallel)\psi_e(z_e)\psi_h(z_h) , \quad (47)$$

where $\psi_e(z_e)$ and $\psi_h(z_h)$ satisfy

$$\left\{-\frac{\hbar^2}{2}\frac{d}{dz_e}\left[\frac{1}{m_e(z_e)}\frac{d}{dz_e}\right]+V_e^{\text{eff}}(z_e) + \frac{\mu_0 E_\parallel}{m_e(z_e)}\right\}\psi_e(z_e)=E_e\psi_e(z_e) \quad (48)$$

and

$$\left\{-\frac{\hbar^2}{2}\frac{d}{dz_h}\left[\frac{1}{m_h(z_h)}\frac{d}{dz_h}\right]+V_h^{\text{eff}}(z_h) + \frac{\mu_0 E_\parallel}{m_h(z_h)}\right\}\psi_h(z_h)=E_h\psi_h(z_h) , \quad (49)$$

with

$$E_\parallel=\frac{\hbar^2\mathbf{k}_\parallel^2}{2m_e(z_e=0)}+\frac{\hbar^2\mathbf{k}_\parallel^2}{2m_h(z_h=0)} \quad (50)$$

and

$$\frac{1}{\mu_0}=\frac{1}{m_e(z_e=0)}+\frac{1}{m_h(z_h=0)} . \quad (51)$$

The transition energy is the sum of the energy eigenvalues of Eqs. (48) and (49) and the band-gap energy, namely,

$$E_T=E_e+E_h+E_G . \quad (52)$$

If the planar relative motion is ignored, namely, $\mathbf{k}_\parallel=\mathbf{0}$, Eqs. (48) and (49) reduce to the single-band effective-mass equations for the electron and the hole,

$$\left\{-\frac{\hbar^2}{2}\frac{d}{dz_e}\left[\frac{1}{m_e(z_e)}\frac{d}{dz_e}\right]+V_e^{\text{eff}}(z_e)\right\}\psi_e(z_e)=E_e\psi_e(z_e) \quad (53)$$

and

$$\left\{-\frac{\hbar^2}{2}\frac{d}{dz_h}\left[\frac{1}{m_h(z_h)}\frac{d}{dz_h}\right]+V_h^{\text{eff}}(z_h)\right\}\psi_h(z_h)=E_h\psi_h(z_h) . \quad (54)$$

The transition energy E_T is calculated by Eqs. (53), (54), and (52). Then the band-offset ratio calculation is performed as follows to demonstrate the band-offset ratio variation due to the choice of the Hamiltonian.

The transition energy between a level in the conduction band and a level in the valence band is first obtained by using the BenDaniel and Duke Hamiltonian with a given band-offset ratio (Q_C^{BDDH}). Then the band-offset ratios for the redistributed Hamiltonian (Q_C^{RH}), the Bastard Hamiltonian (Q_C^{BH}), and the Zhu and Kroemer Hamiltonian (Q_C^{ZKH}) are sought to reproduce the same transition energy as the BenDaniel and Duke Hamiltonian between identical transition levels. This process is repeated for several band-offset ratios and for various transitions. Calculation of the 11 HH, 11 LH, 22 HH, and 22 LH transitions are performed in this paper.

Let Q_C^H be the band-offset ratio of a non-BenDaniel and Duke Hamiltonian; that is, let Q_C^H be Q_C^{RH}, Q_C^{BH}, or Q_C^{ZKH}. And let E_H and E_{BDDH} be the transition energies between identical levels obtained by a non-BenDaniel and Duke Hamiltonian and the BenDaniel and Duke Hamiltonian, respectively. The non-BenDaniel and Duke Hamiltonian band-offset ratio is found by solving, with a given Q_C^{BDDH},

$$E_H(Q_C^H)=E_{\text{BDDH}}(Q_C^{\text{BDDH}}) . \quad (55)$$

An interesting relation between the dependence of Q_C^H on Q_C^{BDDH} and the dependence of E_H on Q_C^{BDDH} can be established below.

Taking derivatives of both sides of Eq. (55) with respect to Q_C^{BDDH}, it follows that

$$\frac{dQ_C^H}{dQ_C^{\mathrm{BDDH}}}=\frac{1}{dE_H/dQ_C^H}\frac{dE_{\mathrm{BDDH}}}{dQ_C^{\mathrm{BDDH}}} . \tag{56}$$

From Eq. (56), $dQ_C^H/dQ_C^{\mathrm{BDDH}}$ and $dE_{\mathrm{BDDH}}/dQ_C^{\mathrm{BDDH}}$ vanish at the same Q_C^{BDDH} if dE_H/dQ_C^H is nonzero and finite at Q_C^{BDDH}. Moreover, $dQ_C^H/dQ_C^{\mathrm{BDDH}}$ and $dE_{\mathrm{BDDH}}/dQ_C^{\mathrm{BDDH}}$ have the same sign if $dE_H/dQ_C^H>0$ for Q_C^H in the range of interest. These behaviors will be further examined with computational results in the next section.

V. NUMERICAL RESULTS AND DISCUSSIONS

It was shown in Sec. II that the potential energy of the BenDaniel and Duke Hamiltonian differs from the effective potentials of the other Hamiltonians by a term caused by the mass dependence on location. If the modified square quantum well illustrated in Sec. III is employed, the effective potential varies with the Hamiltonian used. Thus the solution to the effective-mass equation changes with the Hamiltonian. In Sec. V A, the eigensolutions to various Hamiltonians are calculated in the conduction band.

The band-offset ratio of a quantum well determines the barrier height of the conduction and the valence bands. The shape of the effective potential depends on the Hamiltonian used. Thus both the band-offset ratio and the Hamiltonian affect the transition energies in the conduction and the valence bands. If the transition energy is assumed to be fixed, and the analysis using a particular Hamiltonian is performed to reproduce the same transition energy, then an appropriate band-offset ratio must be incorporated with the chosen Hamiltonian. This relation between the band-offset ratio and the Hamiltonian will be explored in Sec. V B. The transitions investigated include 11 HH, 11 LH, 22 HH, and 22 LH.

For the calculations in both subsections, the dispersive factors of the effective masses of the electron and the heavy and the light holes as well as the dispersive factors of the conduction- and valence-band potential energies are assumed to be equal for simplicity. Namely,

$$\sigma_e=\sigma_{\mathrm{hh}}=\sigma_{\mathrm{lh}}=\sigma_C=\sigma_V=\sigma . \tag{57}$$

The effective-mass equation with vanishing boundary conditions is numerically solved for various Hamiltonians. Note that the differential operator in the left-hand side of Eq. (14) is self-adjoint. A self-adjoint operator $\mathcal{D}$ is an operator which satisfies $\int \phi\mathcal{D}\psi\, dz=\int \psi\mathcal{D}\phi\, dz+$ boundary terms, for arbitrary functions ϕ and ψ. This property facilitates the variational approach of the finite-element method applied to the quantum-well problems. Strictly, the finite-element scheme used in this paper requires that the first derivative of the mass be continuous, namely, that the mass be a C^1 function.[30] Although the modified square quantum well does not exactly satisfy this requirement, the discontinuity given by Eq. (32) is insignificant if the dispersive factor σ is sufficiently small. The profile symmetrically defined by two error functions is, therefore, considered as an approximation of a C^1 function. The magnitude of discontinuity will be noted for the subsequent calculations.

A. Eigensolutions in the conduction band

In this subsection, the conduction-band calculation of a modified square quantum well fabricated from GaAs and $Al_xGa_{1-x}As$ is performed, to explore the effects of the Hamiltonian on the effective potential energy and the eigensolution.

The well width L is taken to be 67.84 Å (24 monolayers of the GaAs lattice[37]). The composition fraction x is 0.3, and the conduction-band-offset ratio Q_C is 0.6. The barrier height of the conduction band V_C^0 is 224.46 meV by Eq. (28), and $\beta_e=0.0249m_0$ by Eq. (29). The calculations are performed with the dispersive factor σ varying from 2.83 (one monolayer) to 14.13 Å (five monolayers).

In Fig. 2, the effective potential profiles for various Hamiltonians are depicted with $\sigma=5.65$ Å (two monolayers). When the redistributed Hamiltonian, the Bastard Hamiltonian, and the Zhu and Kroemer Hamiltonian are expressed in differential forms similar to the BenDaniel and Duke Hamiltonian, the position-dependent effective-mass modifies the real potential energy in the fashion that the lower half of the quantum well is narrowed and the upper half is widened. The deviations of the effective potentials of the non-BenDaniel and Duke Hamiltonians from the BenDaniel and Duke Hamiltonian increase in the sequence of the redistributed Hamiltonian, the Bastard Hamiltonian, and the Zhu and Kroemer Hamiltonian.

The conduction band of the structure calculated in this subsection supports two eigenlevels. The eigenenergies obtained by various Hamiltonians are plotted in Fig. 3 as functions of the dispersive factor. We find that the eigenenergies obtained by different Hamiltonians vary

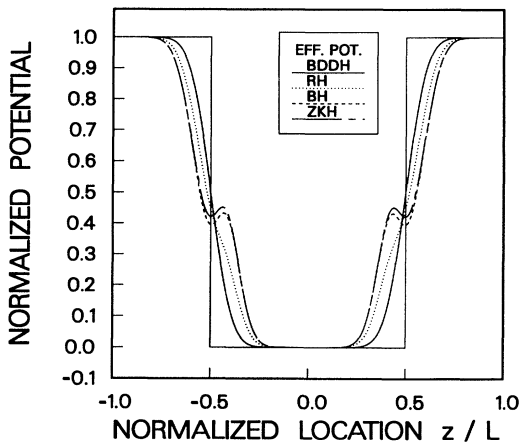

FIG. 2. The effective potentials of the four Hamiltonians are drawn for the electron in the conduction band of a GaAs-$Al_{0.3}Ga_{0.7}As$ quantum well. The effective potentials of the BenDaniel and Duke Hamiltonian (BDDH), the redistributed Hamiltonian (RH), the Bastard Hamiltonian (BH), and the Zhu and Kroemer Hamiltonian (ZKH) are shown in solid, dotted, dashed, and chain-dashed curves, respectively. The potential profiles are normalized by the barrier height of the conduction band (V_C^0), and the dispersive factor (σ) is taken to be two monolayers.

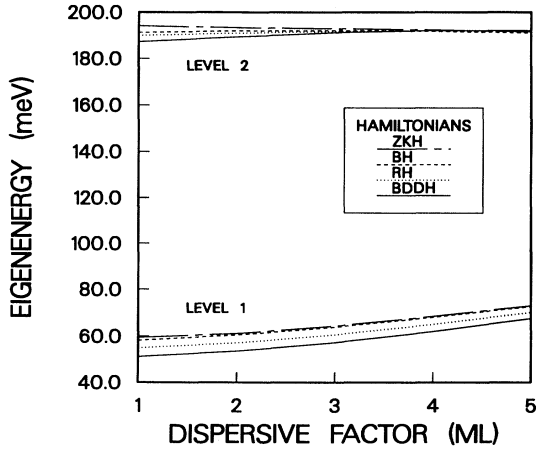

FIG. 3. Depicted are the eigenenergies of the two levels established in the conduction band of the GaAs-$Al_{0.3}Ga_{0.7}As$ quantum well, with a conduction-band-offset ratio of 0.6. The dispersive factor changes from one to five monolayers.

less as the dispersive factor increases. In other words, the choice of the Hamiltonian in analytic work is less important for a smoother profile. Note that the normalized slope discontinuities of the profiles with the dispersive factors of one, two, three, four, and five monolayers are 2.6×10^{-32}, 3.6×10^{-9}, 5.3×10^{-5}, 1.3×10^{-3}, and 5.4×10^{-3}, respectively. It can be seen that, for the quantum well with the width of 24 monolayers, the mass profile with the dispersive factor less than or equal to three monolayers well approximates a C^1 function.

The ground level is more susceptible to the narrowing of the lower half of the quantum well than to the widening of the upper half. The first eigenenergies of the BenDaniel and Duke Hamiltonian, the redistributed Hamiltonian, the Bastard Hamiltonian, and the Zhu and Kroemer Hamiltonian increase in the sequence stated above. As the dispersive factor increases, the lower half of the quantum well becomes narrower. The first energies for all of the Hamiltonians are, therefore, pushed to higher values, as shown in Fig. 3.

For the energy of the second level, there are two competing factors which affect the eigenenergy. The narrowing of the lower half of the quantum well tends to increase the eigenenergy, but the widening of the upper half tends to decrease the eigenenergy. From Fig. 3, it can be observed that, for a fixed dispersive factor which is small enough, the second-level eigenenergies of the BenDaniel and Duke Hamiltonians, the redistributed Hamiltonian, the Bastard Hamiltonian, and the Zhu and Kroemer Hamiltonian increase in the same sequence as the first-level energies. This indicates that, as the dispersive factor is small, the effect of the narrowing of the lower half overwhelms the effect of the widening of the upper half. However, this domination does not persist as the dispersive factor becomes larger. As shown in Fig. 3, the second eigenenergies for the four Hamiltonians are barely distinguishable for the dispersive factor greater than three monolayers.

The competing of the two effects mentioned above also explains the following two features of the second eigenenergy. First, at a fixed dispersive factor, the second eigenenergies obtained by different Hamiltonians vary less than the first eigenenergies. Second, as the dispersive factor increases, the first eigenenergy increases monotonically, but the second eigenenergy remains almost unchanged.

B. Band-offset ratio dependence on the Hamiltonian

The scheme outlined in Sec. IV is numerically realized here to manifest the band-offset ratio dependence on the effective-mass Hamiltonian.

The computation in this subsection is implemented for the GaAs-$Al_{0.3}Ga_{0.7}As$ quantum well with the same parameters as that in the previous subsection, except that the band-offset ratio here becomes a variable, and the dispersive factor is taken to be a constant. The well width L is 67.84 Å (24 monolayers). From Eqs. (29), (37), and (38), $\beta_e=0.0249m_0$, $\beta_{hh}=0.015m_0$, and $\beta_{lh}=0.030m_0$. The dispersive factor σ is taken to be 5.65 Å (two monolayers). The normalized slope discontinuities of the mass profiles of the electron and the heavy and light holes are 3.6×10^{-9}, 2.2×10^{-9}, and 4.3×10^{-9}, respectively.

The 11 HH, 11 LH, 22 HH, and 22 LH transition energies of the BenDaniel and Duke Hamiltonian are depicted in Fig. 4 as a function of its band-offset ratio. The deviations of the transition energies of the non-BenDaniel and Duke Hamiltonians from the BenDaniel and Duke Hamiltonian are plotted in Fig. 5 for the heavy hole, and in Fig. 6 for the light hole. In Fig. 7, the band-offset ratios of the redistributed Hamiltonian, the Bastard Hamiltonian, and the Zhu and Kroemer Hamiltonian necessary

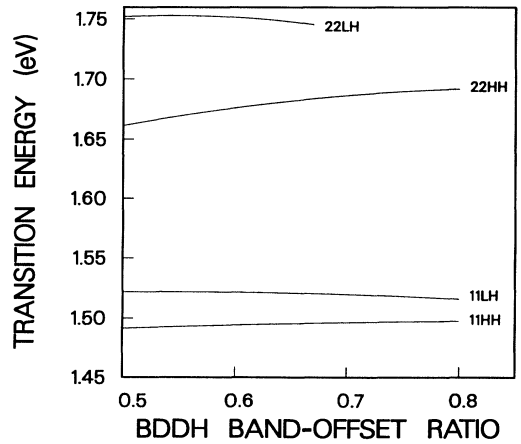

FIG. 4. The energies of the 11 HH, 11 LH, 22 HH, and 22 LH transitions obtained by the BenDaniel and Duke Hamiltonians are drawn vs its band-offset ratio. Curves for the 11 and 22 HH transitions are monotonically increasing, while those for the 11 and 22 LH transitions increase and then decrease. The change rate of the 11 LH transition is so gentle that it is difficult to discern its variation on the graph.

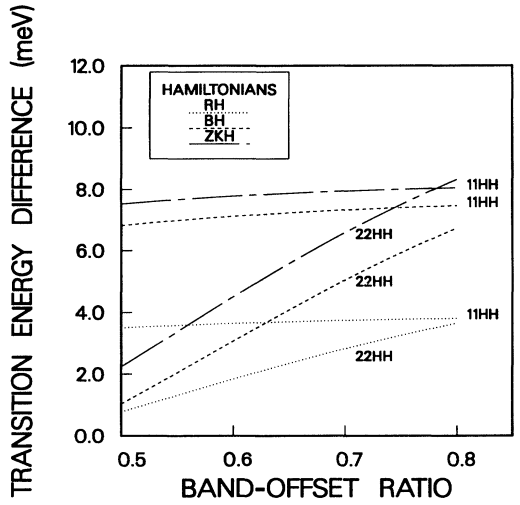

FIG. 5. The transition energy differences of the non-BenDaniel and Duke Hamiltonians from the BenDaniel and Duke Hamiltonian are plotted for the heavy-hole transitions 11 and 22 HH.

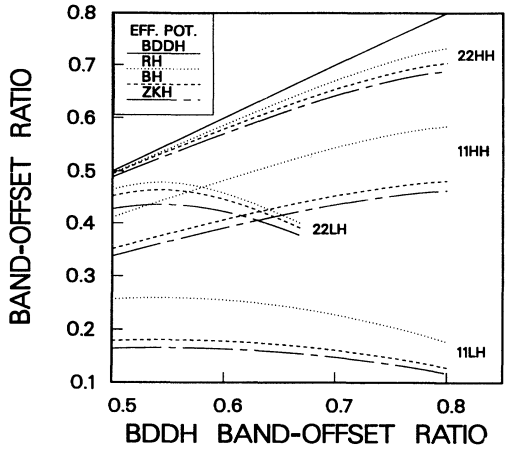

FIG. 7. The band-offset ratios for the four Hamiltonians required to produce the same transition energies between the same levels are plotted vs the BenDaniel and Duke Hamiltonian band-offset ratio. The four transitions investigated are 11 HH, 11 LH, 22 HH, and 22 LH. The 22 LH transition no longer exists when the BenDaniel and Duke Hamiltonian band-offset ratio exceeds 0.67, because the second level of the light hole disappears.

to produce the same 11 HH, 11 LH, 22 HH, and 22 LH transition energies as the BenDaniel and Duke Hamiltonian are drawn versus the band-offset ratio of the BenDaniel and Duke Hamiltonian. In all of the figures, the curves related to the 22 LH transition terminate before the BenDaniel and Duke Hamiltonian band-offset ratio exceeds 0.67, because the valence band supports only one light-hole level at the band-offset ratio greater than 0.67.

In Fig. 4, as the band-offset ratio increases, the large mass difference between the electron and the hole results in the increase of the 11 and 22 HH transition energies. The 11 and 22 LH transition energies first increase and then decrease because the light-hole mass is only slightly larger than the electron.

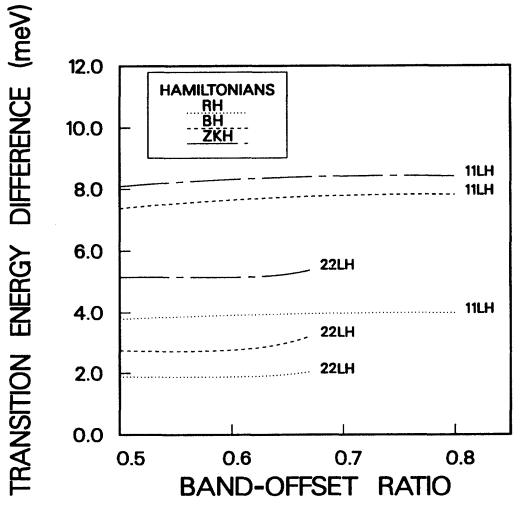

FIG. 6. The transition-energy differences of the non-BenDaniel and Duke Hamiltonians from the BenDaniel and Duke Hamiltonian are plotted for the light-hole transitions 11 and 22 LH.

As shown in Figs. 5 and 6, the energies for a particular transition obtained by different Hamiltonians at a fixed band-offset ratio increases in the same order as in Fig. 3. Because the effective masses of both the heavy and light holes are larger than the electron, the transition energy obtained by the non-BenDaniel and Duke Hamiltonian can be lowered by decreasing the band-offset ratio. If the non-BenDaniel and Duke Hamiltonian band-offset ratio is continually lowered until its energy difference from the BenDaniel and Duke Hamiltonian is compensated for, the same transition energy as the BenDaniel and Duke Hamiltonian is achieved. Consequently, the band-offset ratios of distinct Hamiltonians having the same transition energy between the same levels now run in the reverse order of the transition energy; that is, they increase in the order of the Zhu and Kroemer Hamiltonian, the Bastard Hamiltonian, the redistributed Hamiltonian and the BenDaniel and Duke Hamiltonian, as shown in Fig. 7.

In Fig. 7, we show how band-offset ratios of the non-BenDaniel and Duke Hamiltonians which produce the same 11 and 22 HH transition energies as the BenDaniel and Duke Hamiltonian monotonically increase when the BenDaniel and Duke Hamiltonian band-offset ratio increases. However, the band-offset ratios which produce the same 11 and 22 LH transition energies first increase, and then decrease. These behaviors can be related by Eq. (56) to the transition energy of the BenDaniel and Duke Hamiltonian given in Fig. 4.

From Figs. 4 and 5, it can be seen that the transition energies (especially the 11 HH and 11 LH transitions) are rather insensitive to the band-offset ratio and the Hamiltonian. Hence, the same transition energy can be repro-

duced by somewhat different band-offset ratios, as shown in Fig. 7. Thus an attempt to determine the band-offset ratio from experimental data would involve large inaccuracy.

VI. CONCLUDING REMARKS

By permuting two momentum operators ($\hat{p}$) and two mass operators [$1/\sqrt{m(\hat{z})}$], the BenDaniel and Duke Hamiltonian, the Bastard Hamiltonian, and the Zhu and Kroemer Hamiltonian are reconstructed. Moreover, a redistributed Hamiltonian is suggested by arguments parallel to those which generate the Bastard Hamiltonian. All of these Hamiltonians are expressed in a self-adjoint differential form to facilitate the finite-element analysis.

A square quantum well is modeled by a modified profile which is smoothed at the heterojunctions, to take account of the finiteness of the internal electric field. The modified square quantum well is described by error functions whose first derivatives are normally distributed with a standard deviation, termed a dispersive factor (σ) in this paper.

The effective potential is the sum of the real potential and a term resulting from the mass dependence on the location. The effective potential relies on the Hamiltonian utilized, and its deviation from the real potential increases in the following sequence: the BenDaniel and Duke Hamiltonian, the redistributed Hamiltonian, the Bastard Hamiltonian, and the Zhu and Kroemer Hamiltonian.

In the interpretation of a given spectrum, the Hamiltonian employed in the analysis *cannot* be regarded independently of the band-offset ratio utilized, if the modified profile is used. Furthermore, the band-offset ratio determined by frequently used means of matching calculated transition energies with spectral peaks would be rather inaccurate.

ACKNOWLEDGMENTS

The authors would like to thank Dr. R. B. Darling for his useful comments. This work is supported by the U.S. National Science Foundation and the Office of Naval Research under the Grant Nos. ECS-9158036 and N00014-91-J-1662, respectively.

APPENDIX A: THE CURVES IN FIG. 1

The meanings of the remaining curves in Fig. 1 are interpreted in this appendix. In Fig. 1, the modified square quantum well with the band-offset ratio of 0.5 is sketched. In addition to the potential profiles of the sharp and the modified square quantum wells, the effective potentials of the Zhu and Kroemer Hamiltonian are plotted. In the conduction band, the effective potential of the electron is drawn in a chain-dashed curve. In the valence band, the effective potentials of the heavy and light holes are in dashed and dotted curves, respectively. There are a total of two, three, and two levels for the electron, the heavy hole, and the light hole, respectively. However, only the envelope functions of their first levels are shown in the figure, with line styles same as the effective potentials.

It appears that the effective potential of the heavy hole is not depicted in Fig. 1. In fact, the effective potential of the heavy hole also appears in the plot, but it is so close to the real potential profile that the two potentials cannot be distinguished in the figure. The modification of the potential profile of the electron is usually far greater than that of the heavy hole, because of the order of magnitude difference of their effective masses.

[1]R. Dingle, W. Wiegmann, and C. H. Henry, Phys. Rev. Lett. **33**, 827 (1974).
[2]R. C. Miller, D. A. Kleinman, and A. C. Gossard, Phys. Rev. B **29**, 7085 (1984).
[3]D. A. Kleinman, R. C. Miller, A. C. Gossard, and O. Munteanu, Phys. Rev. B **29**, 3740 (1984).
[4]M. H. Meynadier, C. Delalande, G. Bastard, and M. Voos, Phys. Rev. B **31**, 5539 (1985).
[5]P. Dawson, B. A. Wilson, C. W. Tu, and R. C. Miller, Appl. Phys. Lett. **48**, 541 (1986).
[6]P. Dawson, G. Duggan, H. I. Ralph, K. Woodbridge, and G. W. 't Hooft, Superlatt. Microstruct. **1**, 231 (1985).
[7]W. I. Wang and F. Stern, J. Vac. Sci. Technol. B **3**, 1280 (1985).
[8]D. J. Wolford, T. F. Kuech, J. A. Bradley, M. A. Gell, D. Ninno, and M. Jaros, J. Vac. Sci. Technol. B **4**, 1043 (1986).
[9]J. Menéndez, A. C. Gossard, A. Pinczuk, J. H. English, D. J. Werder, and M. G. Lamont, J. Vac. Sci. Technol. B **4**, 1041 (1986).
[10]G. Duggan, J. Vac. Sci. Technol. B **3**, 1224 (1985).
[11]H. Kroemer, Surf. Sci. **174**, 299 (1986).
[12]J. S. Nelson, A. F. Wright, and C. Y. Fong, Phys. Rev. B **43**, 4908 (1991).
[13]S. H. Wei and A. Zunger, Phys. Rev. B **39**, 3279 (1989).
[14]C. G. Van de Walle and R. M. Martin, Phys. Rev. B **35**, 8154 (1987).
[15]S. Datta, *Quantum Phenomena,* Modular Series on Solid State Devices Vol. 8 (Addison-Wesley, Reading, MA, 1989), Chaps. 1 and 6.
[16]T. Gora and F. Williams, Phys. Rev. B **177**, 1179 (1969).
[17]R. A. Morrow and K. R. Brownstein, Phys. Rev. B **30**, 678 (1984).
[18]D. J. BenDaniel and C. B. Duke, Phys. Rev. **152**, 683 (1966).
[19]G. Bastard, Phys. Rev. B **24**, 5693 (1981).
[20]Q. G. Zhu and H. Kroemer, Phys. Rev. B **27**, 3519 (1983).
[21]A. Chomette, B. Deveaud, M. Baudet, P. Auvray, and A. Regreny, J. Appl. Phys. **59**, 3835 (1986).
[22]O. von Roos, Phys. Rev. B **27**, 7547 (1983).
[23]J. Thomsen, G. T. Einevoll, and P. C. Hemmer, Phys. Rev. B **39**, 12 783 (1989).
[24]R. A. Morrow, Phys. Rev. B **35**, 8074 (1987).
[25]M. G. Burt, Semicond. Sci. Technol. **3**, 739 (1988).
[26]M. G. Burt, Semicond. Sci. Technol. **2**, 460 (1987); **2**, 701(E)

(1987).
[27]R. A. Morrow, Phys. Rev. B **36**, 4836 (1987).
[28]G. T. Einevoll and P. C. Hemmer, J. Phys. C **21**, L1193 (1988).
[29]I. Galbraith and G. Duggan, Phys. Rev. B **38**, 10 057 (1988).
[30]T. L. Li and K. J. Kuhn, J. Comput. Phys. (to be published).
[31]F. Stern and S. D. Sarma, Phys. Rev. B **30**, 840 (1984).
[32]S. Adachi, J. Appl. Phys. **58**, R1 (1985).
[33]P. Lawaetz, Phys. Rev. B **4**, 3460 (1971).
[34]F. Bassani and G. P. Parravicini, *Electronic States and Optical Transitions in Solids,* International Series of Monographs in the Science of the Solid State Vol. 8 (Pergamon, Oxford, 1975), p. 189.
[35]D. S. Chuu and Y. C. Lou, Phys. Rev. B **43**, 14 504 (1991).
[36]D. A. B. Miller, D. S. Chemla, T. C. Damen, A. C. Gossard, W. Wiegmann, T. H. Wood, and C. A. Burrus, Phys. Rev. B **32**, 1043 (1985).
[37]R. F. Pierret, *Advanced Semiconductor Fundamentals,* Modular Series on Solid State Devices Vol. 6 (Addison-Wesley, Reading, MA, 1989), p. 14.